

## MIT Open Access Articles

*Inductance Compensation of Multiple Capacitors With Application to Common- and Differential-Mode Filters*

The MIT Faculty has made this article openly available. **Please share** how this access benefits you. Your story matters.

**Citation:** Pierquet, Brandon J., Timothy C. Neugebauer, and David J. Perreault. "Inductance Compensation of Multiple Capacitors With Application to Common- and Differential-Mode Filters." IEEE Trans. Power Electron. 21, no. 6 (n.d.): 1815–1824.

**As Published:** <http://dx.doi.org/10.1109/TPEL.2006.882901>

**Publisher:** Institute of Electrical and Electronics Engineers (IEEE)

**Persistent URL:** <http://hdl.handle.net/1721.1/87021>

**Version:** Final published version: final published article, as it appeared in a journal, conference proceedings, or other formally published context

**Terms of Use:** Article is made available in accordance with the publisher's policy and may be subject to US copyright law. Please refer to the publisher's site for terms of use.



# Inductance Compensation of Multiple Capacitors With Application to Common- and Differential-Mode Filters

Brandon J. Pierquet, *Student Member, IEEE*, Timothy C. Neugebauer, *Member, IEEE*, and David J. Perreault, *Senior Member, IEEE*

**Abstract**—Capacitor parasitic inductance often limits the high-frequency performance of electromagnetic interference (EMI) filters in both common-mode (CM) and differential-mode (DM) filtering domains. However, these limitations can be overcome through the use of specially-coupled magnetic windings that effectively nullify the capacitor parasitic inductance. This document explores the use of a single coupled magnetic winding to provide inductance compensation for multiple capacitors (e.g., both DM and CM capacitors) simultaneously, reducing the number of coils previously required. The substantial advantages of this method are illustrated both in a proof-of-concept test circuit and in an improved version of an existing EMI filter. The coupling between multiple inductance compensation windings in a single filter enclosure is also investigated.

**Index Terms**—Cantilever model, capacitor parasitic inductance, coupled magnetic windings, electromagnetic compatibility (EMC), electromagnetic interference (EMI), EMI filter, inductance cancellation, inductive coupling, radio frequency interference (RFI).

## I. INTRODUCTION

**E**LECTROMAGNETIC interference (EMI) filters are an important part of many types of electrical equipment, and they play a critical role in meeting requirements for device compatibility. The size and performance of these filters are often limited by their component parasitics, such as the equivalent series inductance of capacitors and the equivalent parallel capacitance of inductors [1]–[12]. These limitations have generated recent interest in methods for compensating parasitics to increase filter performance [5]–[12]. For example, as shown in [5]–[7], coupled magnetic windings can be used to cancel the effects of capacitor parasitic inductance. Inductance cancellation windings can be used to reduce the filter volume and cost and/or increase its attenuation performance.

Conventionally, inductance cancellation windings have only been used with a single capacitor. In a filter designed for both common-mode (CM) and differential-mode (DM) filtering, this

Manuscript received November 2, 2005; revised March 3, 2006. This work was supported by the Office of Naval Research Grant N00014-02-1-481, and by the Air Force Research Laboratory through a National Defense Science and Engineering Graduate Fellowship. Recommended by Associate Editor P. Tenti.

B. J. Pierquet and D. J. Perreault are with the Laboratory for Electromagnetic and Electronic Systems, Massachusetts Institute of Technology, Cambridge, MA 02139 USA.

T. C. Neugebauer is with the Charles Stark Draper Laboratory, Massachusetts Institute of Technology, Cambridge, MA 02139 USA (e-mail: pierquet@mit.edu).

Digital Object Identifier 10.1109/TPEL.2006.882901

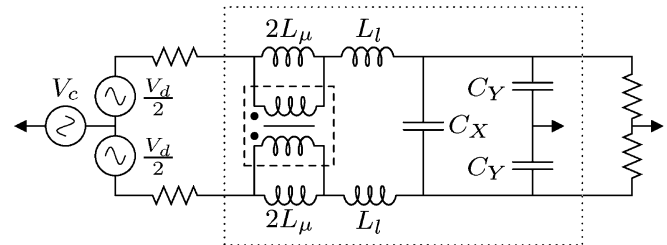


Fig. 1. Simple EMI filter circuit shown with representative source and load networks for performance evaluation. Some parasitic elements (such as capacitor equivalent series inductance) are not shown explicitly.

requires a number of windings to be used to compensate all capacitors. The simple EMI filter in Fig. 1 contains three capacitors: two line-to-common, and one line-to-line.

The goal of this document is to introduce the use of a single coupled magnetic winding to compensate for the effects of the parasitic inductance of two discrete capacitors, thereby saving precious space and added cost. Section II outlines the motivation for applying this concept to EMI filters, and demonstrates its application in experimental test cases. Section III follows with an application of the method to improve an existing EMI filter. Section IV provides an analytic basis for the observed performance improvements, and Section V concludes the paper.

## II. MULTIPLE ELEMENT INDUCTANCE COMPENSATION

### A. Motivation

To understand why the use of a single magnetic winding to compensate for parasitics of two capacitors is of particular value in EMI filtering, consider the structure and operation of an EMI filter. Fig. 1 shows the basic structure of an EMI filter designed to attenuate both CM and DM signals, along with representative source and load networks for performance evaluation. This circuit can be analyzed by separating its CM and DM responses and treating these equivalent circuits as if they were independent [2]. The CM and DM equivalent circuits are shown in Fig. 2.

Now, if the circuit of Fig. 1 is augmented with inductance cancellation coils for each capacitor, the circuit in Fig. 4 is generated. In this new figure, the differential capacitor  $C_X$  is fitted with two inductance cancellation coils instead of only one to preserve circuit symmetry. Past work [5] has shown this to be as effective as a single coil, and Fig. 3 shows a photograph of this where the inductance cancellation windings are fabricated on a PCB.

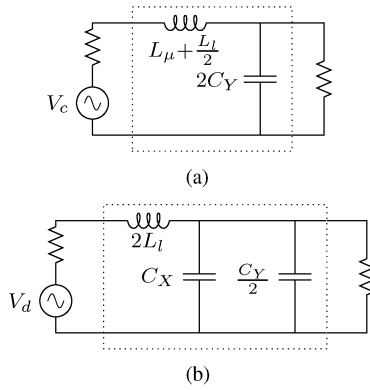


Fig. 2. Models for the simple EMI Filter circuit of Fig. 1, decomposed into CM and DM portions. (a) CM. (b) DM.

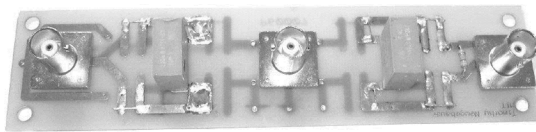


Fig. 3. Test circuit with balanced inductance cancellation windings implemented in the printed circuit board. Performance of this filter has been previously shown [5].

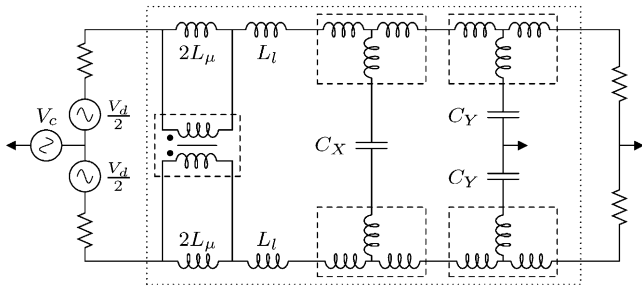


Fig. 4. Simple EMI Filter circuit from Fig. 1 with balanced inductance cancellation of each capacitor.

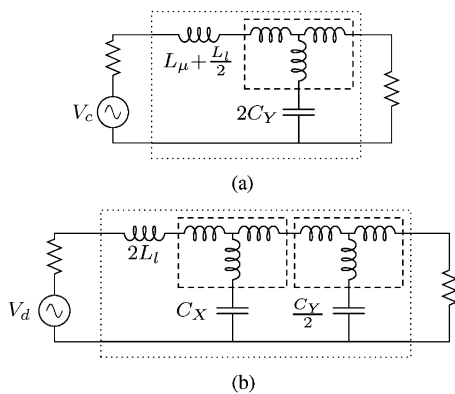


Fig. 5. Simple EMI Filter circuit with balanced inductance cancellation of each capacitor, decomposed into CM and DMs. (a) CM. (b) DM.

It is desirable to implement the cancellation windings in a balanced fashion to avoid inserting an unbalanced circuit element within the otherwise well-balanced system (Fig. 5). Without balancing the series inductances on both sides of the capacitor, a

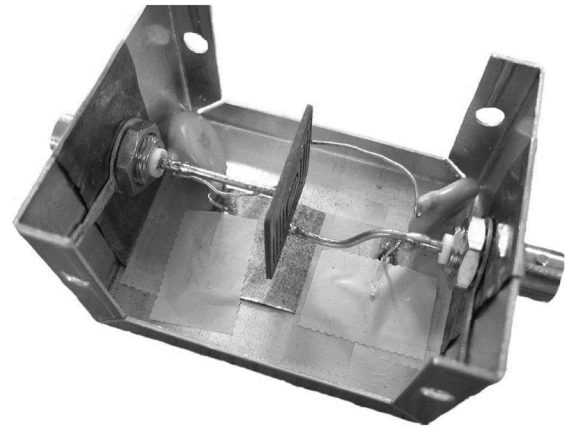
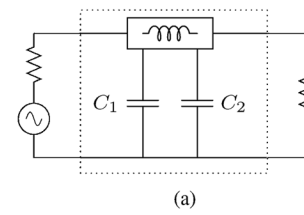


Fig. 6. Test filter for inductance compensation of two Panasonic ECK-ATS472ME6 4700 pF ceramic capacitors using a single magnetic winding. (a) Schematic. (b) Physical layout.

cross coupling between the DM and CM signal sources would result. By avoiding this coupling, the CM and DM circuit equivalents remain straightforward, as illustrated in Fig. 6(a) and (b).

As shown in Fig. 4, the construction of an EMI filter with full, balanced inductance cancellation would require four magnetically coupled windings when constructed using the previously established method. These windings occupy additional space within the filter, and if placed in close proximity may exhibit secondary effects from magnetic coupling, complicating the design. The effects of coupling are investigated more thoroughly in Section II-C. Given these limitations, it would be a considerable improvement if the number of required windings could be reduced by utilizing a single winding to provide appropriate inductance compensation for two capacitors.

### B. Implementation

To show experimentally that the use of a single inductance cancellation coil for two capacitors is feasible, a simple test filter was created with a planar winding mounted with EMI filter capacitors inside a shielded enclosure. Fig. 6 shows the filter along with the two Panasonic ECK-ATS472ME6 4700pF Y2 class ceramic capacitors used. This test filter does not directly examine CM and DM testing, however it does provide a straightforward example how a single coil can support the compensation of inductance for two capacitors. A dimensioned line-art drawing of the coil, which was cut using an OMAX abrasive-jet cutter from a single piece of 1mm thick copper, is shown in Fig. 7. Based on simulation results from FastHenry [13], the coil itself has a maximum series inductance of 393.0 nH, and a maximum equivalent shunt-path inductance of  $-63.2$  nH when used for single element inductance cancellation (in the magnetic winding

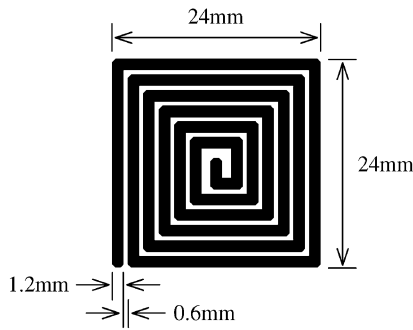


Fig. 7. Illustration of the planar winding used in the test filters of Section II, fabricated from 1mm thick copper. The total series-path inductance based on simulation is 393.0 nH, and the maximum equivalent shunt-path inductance for a single element is  $-63.2$  nH (in the magnetic winding T model).

T model). It should be noted that this coil was intentionally designed to be far over-sized for the amount of cancellation required; this was to allow for maximum flexibility in testing.

The procedure outlined here was developed for tuning the filter response of the two capacitors, and is one way a high performance filter response can be determined. Initially, the connection of capacitor  $C_1$  is tuned to optimally cancel its parasitic inductance. This can be done by adjusting the connection point of the capacitor on the winding while observing the filter attenuation (e.g., with a network analyzer), and/or using methods associated with previously described techniques in [6]. Once its optimal position is found, the position of the capacitor is fixed. Following this, the connection of capacitor  $C_2$  is tuned (with capacitor  $C_1$  in place) to find an optimal filter response. This gives one possible combination of capacitor locations on the coupled winding that results in a high performance filter characteristic.

Experimental results for this test system are shown in Fig. 8, with data taken from an Agilent 4395A network analyzer which provides 50- $\Omega$  source and load impedances. Insertion gain measurements were made in accordance with those used to evaluate inductance cancellation performance in [5], [6] to allow for direct performance comparison. When tuning the response with only  $C_1$ , two measurements were taken for comparison: one with the capacitor connected directly at the input (source-side) terminal providing no cancellation, and one where the capacitor was connected to the cancellation coil at a location where the output response was optimal. The same approach was taken when tuning the response for the combination of  $C_1$  and  $C_2$ :  $C_2$  was connected either directly at the filter output (load-side) terminal or at a position optimizing the filter response with both capacitors.

The characterization results of the filter attenuation performance clearly show a dramatic improvement (as much as 35 dB at high frequency) from the case where no compensation is provided (both not cancelled) to the case where inductance compensation is provided for both capacitors (both cancelled). These results demonstrate that a single coupled magnetic winding can be used to provide inductance compensation for two capacitors, with dramatic performance improvement at high frequencies.

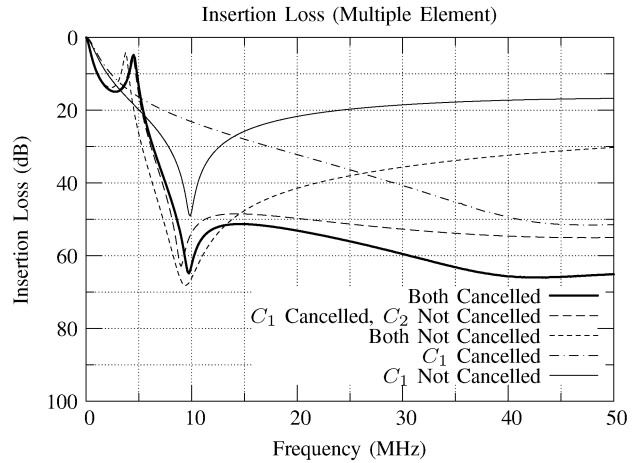


Fig. 8. Measured results from the test filter in Fig. 6 showing the performance of multiple-element inductance compensation.

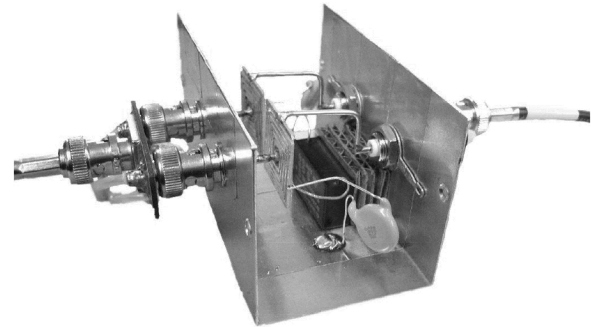


Fig. 9. Filter for investigation of CM and DM coupling between inductance compensation windings.

### C. Coupling of Multiple Windings

When physically placing multiple magnetic windings in close proximity, linked magnetic flux between the windings can affect the predicted performance in various ways [8]. Thus, the implementation of multiple cancellation windings in a single filter may affect the inductance cancellation and filter performance. Here the effects of mutual coupling are explored when two coils are used to provide balanced inductance cancellation for both CM and DM capacitors.

Two additional filters (using the same windings shown in Fig. 7) were created to test two coil configurations having different magnetic coupling directions. In addition to a pair of line-to-ground (Y) capacitors (Panasonic ECK-ATS472ME6) for CM filtering, these test filters incorporate a Rubycon 250MMCA334KUV class X2 line-to-line capacitor for DM filtering. Fig. 9 is a photo of one of the filters, and shows its internal layout. Figs. 10 and 11 show the filter configurations and illustrate the difference between the two winding orientations.

Windings placed in the same direction each throw flux in a way which opposes the flux of its paired winding for CM currents, reducing each winding’s effective inductance. In the case of the windings oriented in the opposite direction, the flux from

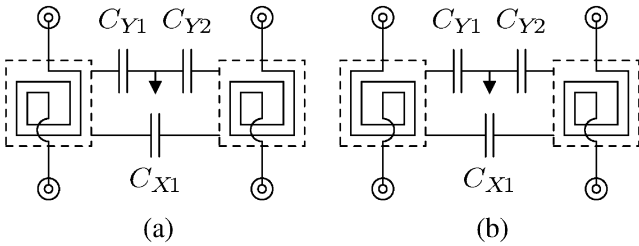


Fig. 10. Two orientations of coupled inductance compensation coils. The coils are of the type shown in Fig. 7.  $C_{Y1}$  and  $C_{Y2}$  are Panasonic ECK-ATS472ME6,  $C_{X1}$  is a Rubycon 250MMCA334KUV. The two circuits only differ with respect to mutual coupling among the coils. (a) Same direction. (b) Opposite direction.

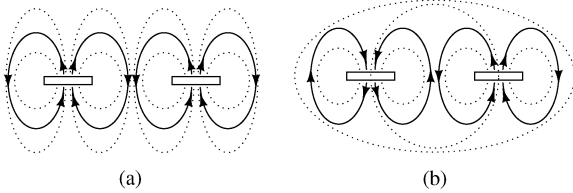


Fig. 11. Flux patterns for CM operation of the two magnetic winding configurations of Fig. 10. Windings oriented in the same direction generate flux in a way which opposes the flux of the paired winding for CM currents. Windings oriented in the opposite direction generate fluxes which reinforce each other, providing a coupling direction like that of a CM choke. (a) Same direction. (b) Opposite direction.

each winding is reinforced by the other for CM currents, providing a coupling direction like that of a CM choke, and increasing each winding's effective inductance.

The tuning procedure used here is similar to the one used in the two-capacitor case in Section II-B. Initially, the connections of capacitors  $C_{Y1}$  and  $C_{Y2}$  are tuned simultaneously in the CM case to compensate for their parasitic inductances (while retaining a balanced configuration). Once the optimal positions are found, the positions of the capacitors are fixed. Following this, the capacitor  $C_{X1}$  is tuned in the DM case by moving its connections on both coils symmetrically to find an optimal output response. Tuning is carried out in this order because ideally the addition of the DM capacitor does not affect the CM response, while the reverse would not necessarily be true.

The experimental setup for calibration and measurement of the CM and DM filter performances are taken from [14], with signal generation and measurement performed by the same Agilent 4395A Network Analyzer as in Section II-B, with Mini-Circuits 180° power splitters (models ZSCJ-2-1 and ZSCJ-2-2) for dividing its output into differential signals, and custom-made CM splitters.

In both winding configurations the target frequency for optimization was 30 MHz, with measurements shown up to 40 MHz. The two orientations possess similar optimized filtration performance, seen in the thicker traces of Fig. 12. The thinner traces in show additional measurements from intermediate steps in the tuning process.

The results show that in both winding orientations an equivalent inductance compensation improvement can be achieved for both the CM and DMs. This allows the orientation of the windings to be selected based on other factors (e.g., based on mag-

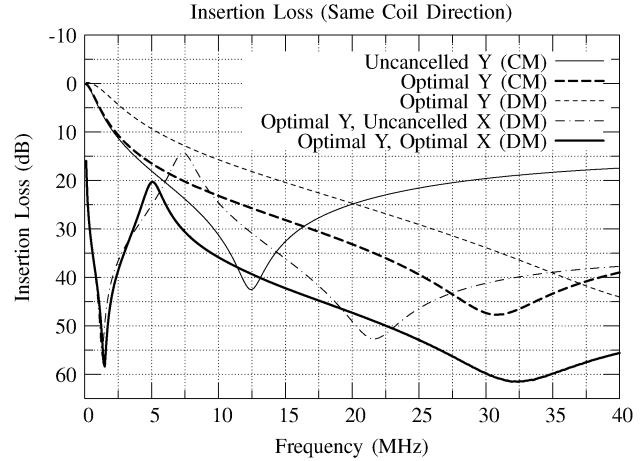


Fig. 12. Measured results from the coupled inductance compensation winding orientations of Fig. 10, including both CM and DM measurements.

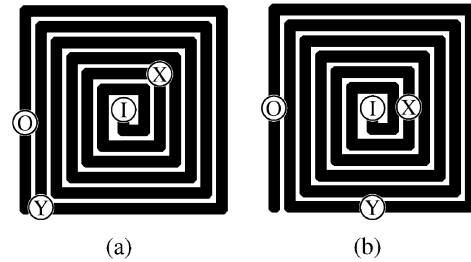


Fig. 13. Connection locations of capacitors corresponding to the results in Fig. 12. Only one winding of each pair is shown, the connections made to the other winding are symmetric.  $X$  represents the connection location of  $C_{X1}$ ,  $Y$  represents the corresponding  $C_{Yn}$  connection location for that winding,  $I$  is connected to the input of the filter, and  $O$  represents the connection to the filter output. (a) Same direction. (b) Opposite direction.

netic coupling with more dominant circuit parasitics). While the winding orientation does not influence the final optimized response in these filters, how each winding orientation achieves this optimum is slightly different. In Fig. 13, the connection locations for the filter capacitors are shown, corresponding to the optimal CM and DM filter response from Fig. 12.

Due to the coupling in the CM, the connection for the  $C_{Yn}$  capacitor was closer to an end terminal on the winding in the opposite direction orientation than in the same direction orientation. Effectively, in the CM, the opposite direction orientation has a marginally higher inductance-per-turn than the same direction orientation, and thus requires a slightly reduced number of turns to achieve the same performance.

Even with the the windings in close proximity, the effects of magnetic coupling on the inductance compensation are minimal. In more extreme cases where the coupling is significantly higher, the observed effects may become more pronounced. Even in this case, however, an equivalent performance should be achievable given properly sized windings.

### III. APPLICATION TO COMMERCIAL EMI FILTER

Having shown in the previous section that a single inductance cancellation winding can be used with two capacitors to improve filtration performance, and that the coupling orientation of multiple windings in a single filter does not adversely affect

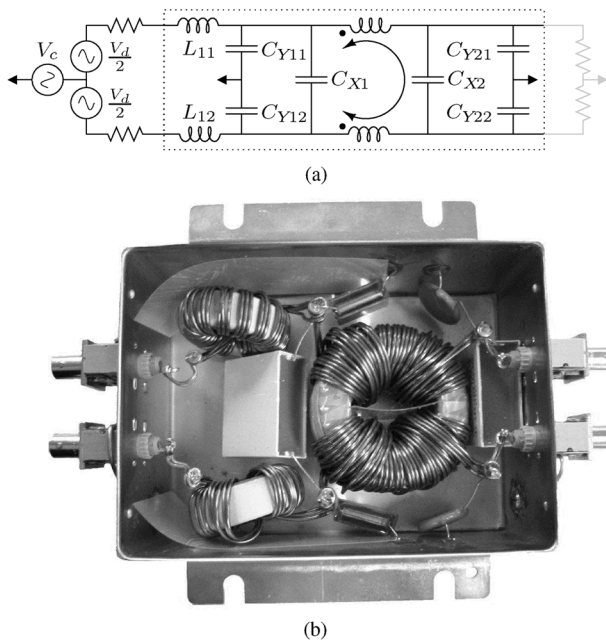


Fig. 14. Original commercial EMI filter.  $L_{11}$ ,  $L_{12}$  are 15- $\mu\text{H}$  wound toroidal inductors,  $C_{Y11}$  and  $C_{Y12}$  are Rifa PME-271 47-nF film capacitors,  $C_{X1}$  and  $C_{X2}$  are Vishay Roederstein F1772-522-2030 2.2- $\mu\text{F}$  film capacitors,  $C_{Y21}$  and  $C_{Y22}$  are 15-nF ceramic capacitors, and the CM choke has a measured leakage inductances of 30.2  $\mu\text{H}$  and a magnetizing inductance of 4.45 mH. (a) Schematic. (b) Physical layout.

potential inductance compensation, the use of multiple element inductance compensation in the context of CM and DM EMI filter is examined. A commercially-available filter is used as a starting point.

Fig. 15(a) and (b) show the schematic and physical views of the filter, which is rated for up to 250 V and 25 A of 50–60 Hz alternating current. The large (15  $\mu\text{H}$ ) series inductors  $L_{11}$  and  $L_{12}$  are particularly bulky, heavy, and expensive components of the commercial filter, and it would be desirable to eliminate them provided that filter performance is preserved. The series inductors were removed to provide working space for installing the inductance cancellation windings, and to provide an opportunity to offset their removal through use of the much smaller cancellation windings. Fig. 16(a) and (b) show the modified schematic and physical layout of the filter with the inductance cancellation windings installed. Additionally, Fig. 16 shows the folded design of the inductance cancellation coil used in this filter. As with the previous coil in Figs. 7 and 16 was cut with an abrasive-jet cutter, using 2-mm thick copper for enhanced current carrying capacity. The flat winding structure is folded at the center of its longest side to form a square one-piece two-layer winding with Mylar tape used as insulation between the layers. Based on simulation results, the coil is estimated to have a series inductance of 288.3 nH, and a maximum equivalent shunt-path inductance of  $-81.2$  nH when used for single element inductance cancellation (in the magnetic winding T model). As in the previous test filters, the coil is purposefully over-designed for the required inductance cancellation to allow for additional design flexibility and testing.

CM and DM measurements were taken of the unmodified filter, as well as an intermediate step before the inductance cancellation windings were installed. In this intermediate step, the

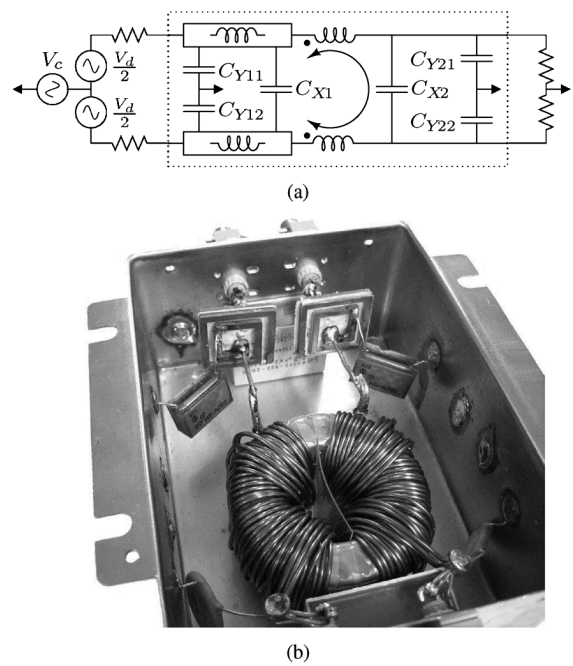


Fig. 15. Modified version of the EMI filter in Fig. 14 with  $L_{11}$  and  $L_{12}$  removed, and two inductance compensation windings installed. (a) Schematic. (b) Physical layout.

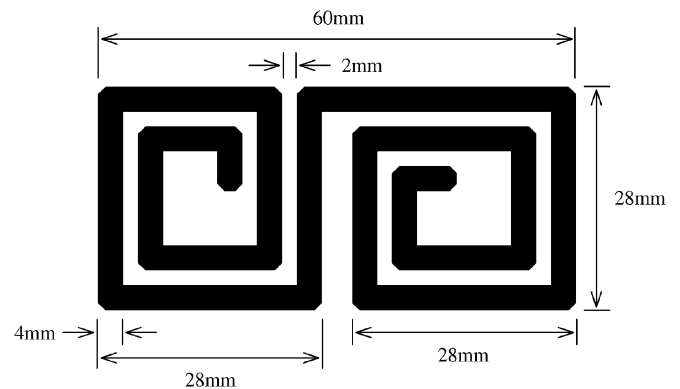


Fig. 16. Illustration of folded winding used for inductance compensation in the EMI filter of Section III, fabricated from 2-mm thick copper. When folded, the total series inductance is 288.3 nH, and the maximum equivalent shunt-path inductance for a single element is  $-81.2$  nH (in the magnetic winding T model).

large inductors  $L_{11}$  and  $L_{12}$  were removed and straight, solid 14ga wire was installed in their place. This configuration, referred to here as without series inductor, was used as a baseline comparison for improvements based on inductance cancellation.

The tuning procedure outlined here is the same as the one used in Section II-C, and was developed for tuning the filter response due to the CM and DM capacitors. Initially, the connections of CM capacitors  $C_{Y1}$  and  $C_{Y2}$  are tuned simultaneously to compensate (in a symmetric fashion) for their parasitic inductances. Once the optimal positions are found, the capacitors are permanently attached to their respective windings. Following this, the DM capacitor  $C_{X1}$  is tuned by moving its connections on both coils symmetrically to find an optimal output response.

This order of tuning makes sense: the CM and DM capacitors do not impact system performance in the same way. In Fig. 6(a),

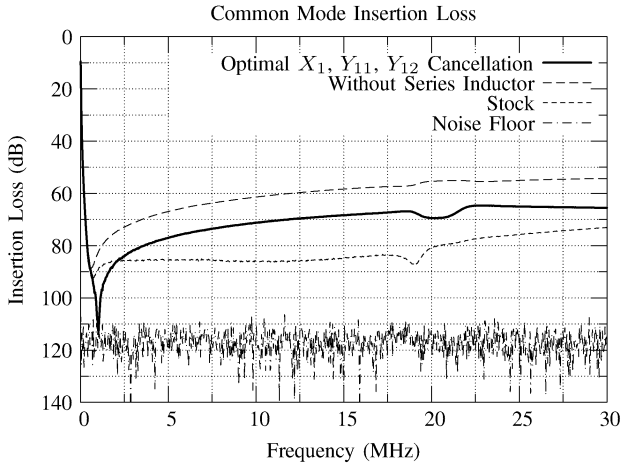


Fig. 17. Performance comparison of the commercially-available EMI filter in Fig. 14 and the modified version in Fig. 15, showing performance both without and with inductance compensation.

it can be seen that the CM equivalent circuit is not influenced by the DM capacitance (or the inductance cancellation, other than through the fixed series inductance introduced by the winding); the CM filtration operates as if the DM capacitor were an open circuit. However, the DM filtration is dependent on the CM capacitance and inductance cancellation. This means that if the inductance compensation for the CM capacitance is optimized first, the inductance compensation for the DM capacitor can be tuned subsequently without influencing the CM performance.

The results of the completed tuning are shown in Fig. 17 along with the stock and baseline filter configurations. It should be noted that tuning of both the CM and DMs is based on compromises between high and low frequency performance. This particular “optimal” output response chosen here may not be the highest achievable performance for a particular range of frequencies of interest (Fig. 18).

The results of incorporating the inductance cancellation coils reveal a dramatic improvement in the filtration performance for both the CM and DM responses over the baseline (stock filter with  $L_{11}$  and  $L_{12}$  removed, labeled as without series inductor). The CM shows improvement across its full range, and the DM shows substantial improvement over its full range except for the small resonance around 2 MHz. (This small resonance is caused in part by the capacitor-inductor-capacitor  $\pi$ -section formed with the two capacitors attached to the inductance compensation winding in the DM, and can be reduced by fabricating a winding with lower series inductance than the over-sized one used here.)

The CM performance with inductance compensation is somewhat worse ( $\sim 10$  dB) than that of the stock filter (with large inductors  $L_{11}$  and  $L_{12}$ ), while the DM performance is comparable. More importantly, the performance with the inductance cancellation windings exceeded the commercially-published performance specification of the stock filter (not shown), without requiring the large, expensive series inductors of the stock filter.

The results from this commercial EMI filter, as well as those from the test filters in Section II, show clearly that a single magnetically coupled winding can provide effective inductance

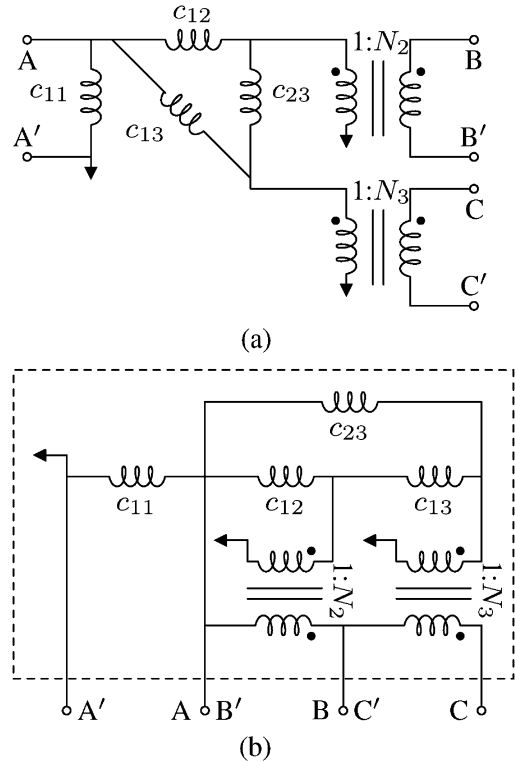


Fig. 18. Three-port extended cantilever models. (a) General configuration. (b) Tapped inductor configuration.

compensation for two capacitors. Moreover, it is demonstrated that the performance of a commercial filter design can be preserved at lower component weight and cost through use of the proposed approach. It is anticipated that further substantial design improvements could be achieved in a filter expressly designed to take advantage of the inductance compensation method proposed here.

#### IV. ANALYTIC FORMULATIONS

In this section, an analytical basis is sought for the proposed method of compensating for the inductance of two capacitors using a single coupled magnetic winding. It is derived from an extension of the methods used to analyze single-capacitor inductance cancellation techniques. The predictions of this method are then compared to measured results to illustrate its usability.

##### A. Extended Cantilever Model

Analysis of inductance cancellation windings with a single capacitor is relatively straightforward since a twoport transformer model of the windings is used, which has only three independent terms. The number of independent terms needed to completely describe coupled magnetics with  $n$  terminals is given by  $n(n+1)/2$  [15], which grows as the square of  $n$ .

Adding to the complexity is the fact that many models for multiple winding transformers either do not adequately model the complete transformer behavior, or have poor correlation and numeric conditioning to attempted measurements of model parameters from terminal characteristics [16], [17]. One model that is effective, and well conditioned for experimental parameter extraction, is the extended cantilever model [15], [16].

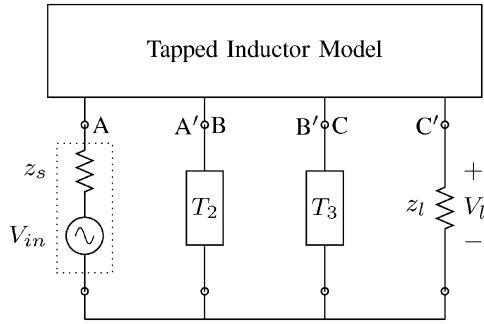


Fig. 19. Shared-terminal three-port circuit for use with the extended cantilever model tapped-inductor configuration of Fig. 19.  $T_2$  and  $T_3$  represent the (inductive) high frequency impedances of the capacitors.

The extended cantilever model of a coupled system yields an equivalent circuit with directly measurable parameters and provides a direct mapping between circuit parameters and the inductance matrix parameters. It is also well conditioned numerically when dealing with small leakage fluxes or high coupling factors. The extended cantilever circuit model for a three-port system is shown in Fig. 19, with circuit parameters related to impedance matrix parameters as follows:

$$Z = sL \quad (1)$$

$$B = \begin{bmatrix} Z_{11} & Z_{12} & Z_{13} \\ Z_{21} & Z_{22} & Z_{23} \\ Z_{31} & Z_{32} & Z_{33} \end{bmatrix}^{-1} \quad (2)$$

$$N_k = \frac{Z_{1k}}{Z_{11}} \quad (3)$$

$$c_{11} = Z_{11} \quad (4)$$

$$c_{ij} = \frac{1}{N_i N_j b_{ij}} \quad (5)$$

where  $b_{ij}$  is the  $(i, j)$ th element of  $B$ .

It should be clarified that the notation used to indicate the impedance matrix  $Z$  is representative of only the reactive component of  $Z$  due to the equivalent inductance; the extended cantilever model in [15] is formulated only with consideration to inductances. An extension which allows for full Laplace domain circuit elements can be found in [18], [19], however in the idealized case considered here, parasitic resistances and capacitances are assumed to be negligible.

### B. Three-Port Analysis

Fig. 19 shows the application of the extended cantilever model to a center-tapped winding with two tap points. Fig. 19 shows additional circuit connections used for finding the system transfer function. The full transfer function for the system is given in Appendix I, and truncated versions are utilized in this section where appropriate.

By analogy to the case of inductance cancellation for a single capacitor, we desire to find conditions that drive the transfer function from the input source to the output voltage to zero (or close to zero). In finding where the transfer function goes to zero, conditions must be found where both the numerator becomes zero, and the denominator remains finite and non-zero. Starting from the numerator of the full transfer function in (10) from Appendix I, setting it equal to zero, refactoring, and di-

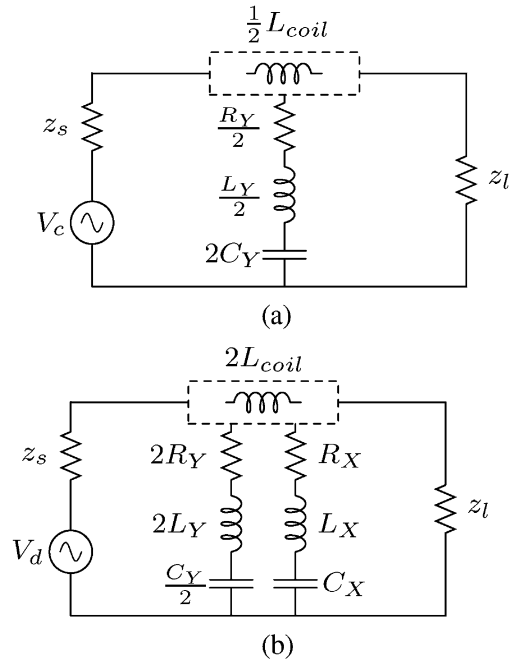


Fig. 20. CM and DM equivalent circuits used to simulate the filters in Section II-C. (a) CM. (b) DM.

viding by the non-zero value of  $z_l$ , a condition is found in which a zero in the numerator can be generated

$$0 = Z_{13}(Z_{12} + Z_{23} + Z_{13} + Z_{22}) - (T_2 - Z_{12} - Z_{13})(T_3 - Z_{13} - Z_{23}). \quad (6)$$

This result, considered by itself, provides a number of terms that can be adjusted to satisfy the equality. However, in the case of CM and DM filtering there are additional constraints that must be considered.

### C. CM and DM Optimization

As described previously in Sections II-C and III, in an EMI filter the CM and DM capacitors do not impact system performance in the same way: the CM filtration operates as if the DM capacitor were an open circuit, while the DM filtration is dependent on the CM capacitance and its inductance cancellation. To find the optimal cancellation for the CM capacitor, the transfer function in (10) is considered at the limit where  $T_3 \rightarrow \infty$  (the DM capacitance is a virtual open circuit for CM signals)

$$H(s) = \frac{(T_2 - Z_{13} - Z_{12})z_l}{\dots} = 0. \quad (7)$$

From this result, it is shown that if  $T_2 = Z_{12} + Z_{13}$ , then full cancellation in the CM can be achieved. With the CM cancellation constraint met, the result is then inserted back into the original transfer function in (10) to find the constraint placed on the DM compensation

$$H(s) = \frac{Z_{13}(Z_{12} + Z_{23} + Z_{13} + Z_{22})}{\dots} = 0. \quad (8)$$

The numerator of this result contains no terms of  $T_3$  in which to tune in comparison to the terms of the impedance



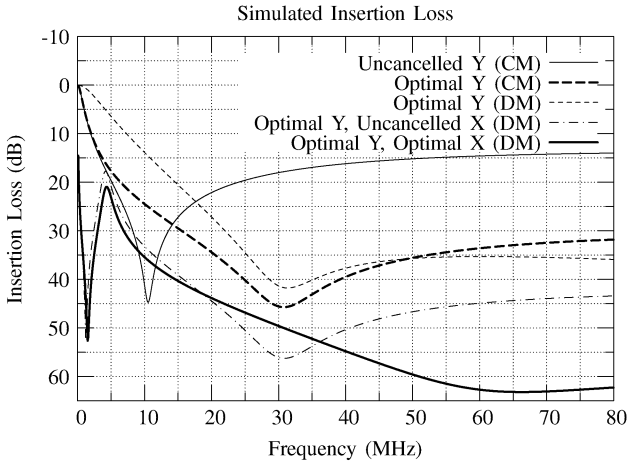


Fig. 21. Simulated results for the filters in Section II-C, using the circuits shown in Fig. 20. Note the different frequency range than in Fig. 12.

matrix. Additionally, the terms of the impedance matrix in a cylindrically or concentrically wound coil configuration are positive, preventing simple geometries from creating a zero in the transfer function. If DM compensation is to be achieved, this result seems to provide no opportunity for the transfer function to become zero, save for the possibility of making  $Z_{13} = 0$ . In the case where  $Z_{13}$  can be made zero, the transfer function denominator would remain finite and non-zero, representing a possible condition to generate a zero for the transfer function, if the structure can be arranged to provide it.

Another consideration may apply in this case. In past work [6], it was shown that depending on the frequency range of interest, filter performance, even with imperfect cancellation, may be perfectly adequate for practical purposes. With imperfect cancellation, a new term  $\Delta_2$  can be defined to be the effective residual shunt-path impedance of the capacitor. More specifically,  $\Delta_2 = T_2 - (Z_{12} + Z_{13})$ . If this is substituted into the general condition in (6), and with the resulting equation rearranged, (9) results. This provides a relation where  $Z_{13}$  is not explicitly required to be zero for the transfer function to become zero

$$0 = Z_{13}(T_2 + Z_{22} + Z_{23}) - \Delta_2(T_3 - Z_{23}). \quad (9)$$

Hence, one may gain good performance in both CM and DM by realizing substantial (but not perfect) cancellation in CM to benefit DM performance (Figs. 21 and 22).

#### D. Simulation and Model Validation

To validate the model and transfer function analysis, the CM and DM filters constructed in Section II-C are used as the basis for simulation, excluding the coupling between the two coils. Each of the measurements presented in the section is simulated here using the model developed, to allow comparison to the experimental results.

To simulate both CM and DM responses, the equivalent circuit models for each model are constructed. These equivalent circuit models, shown in Fig. 20, include the inductance compensation windings, as well as the equivalent series resistance and equivalent series inductance of each capacitor. This allows

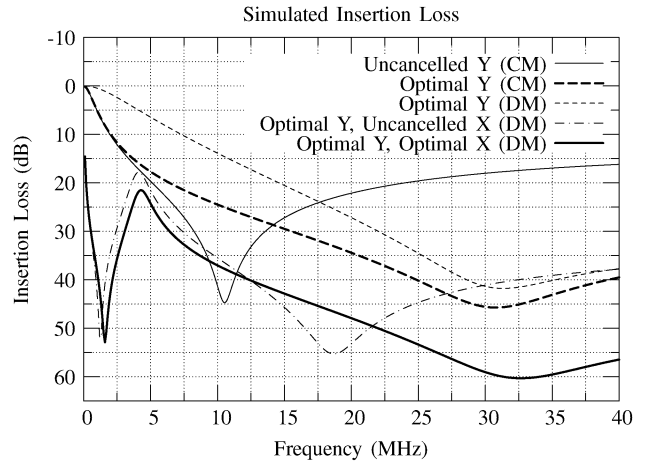


Fig. 22. Simulated results for the filters in Section II-C, using the circuits shown in Fig. 20 with additional DM Y capacitor inductance.

for the direct use of (10) from the Appendix, the transfer function of the circuit in Fig. 19.

In the simulation, both the line-to-ground (Y) capacitor (Panasonic ECK-ATS472ME6) and the line-to-line (X) capacitor (Rubycon 250MMCA334KUV) are modeled with first-order equivalent series resistance, equivalent series inductance, and bulk capacitance. The nominal value of capacitance, along with the measured values of inductance and resistance, are used in the model of each capacitor. The Y capacitor parameters are  $R_Y = 200 \text{ m}\Omega$ ,  $L_Y = 48.6 \text{ nH}$ ,  $C_Y = 4700 \text{ pF}$ ; the X capacitor parameters are  $R_X = 50 \text{ m}\Omega$ ,  $L_X = 49.4 \text{ nH}$ ,  $C_X = 330 \text{ nF}$ . The source ( $z_s$ ) and load ( $z_l$ ) impedances match those of the network analyzer,  $50 \Omega$ . The coil used in the test filters, shown in Fig. 7, is represented by the inductance matrix  $L_{\text{coil}}$ , which is obtained using the numerical inductance calculation tool FastHenry

$$L_{\text{coil}} = \begin{bmatrix} 36.52 & 42.62 & 0.236 \\ 42.62 & 224.6 & 8.089 \\ 0.236 & 8.089 & 5.262 \end{bmatrix} \text{ nH}.$$

For CM  $T_3$  is set to  $1 \text{ M}\Omega$  to approximate an open circuit, and  $T_2$  is set to the effective impedance of the Y capacitor,  $Z_{Y_{\text{CM}}} = 1/2[R_Y + (j\omega C_Y)^{-1} + j\omega L_Y]$ . For the DM simulation, the effective impedance of the Y capacitor is different. With the two capacitors in series, the effective impedance of the Y capacitor is different. With the two capacitors in series, the effective impedance, and thus  $T_2$ , now becomes  $Z_{Y_{\text{DM}}} = 2[R_Y + (j\omega C_Y)^{-1} + j\omega L_Y]$ . The effective impedance of the X capacitor is  $Z_{X_{\text{DM}}} = R_X + (j\omega C_X)^{-1} + j\omega L_X$ , the value used for  $T_3$ .

The results of the CM and DM simulations are shown in Fig. 21. Comparing the simulation results to the experimental data in Fig. 12, the DM results do match in an absolute sense. The Optimal Y (DM) simulation is roughly between two measured coupling cases, which is understandable given coupling between the coils is not modeled. However, the addition of the X capacitor in the Optimal Y, Uncanceled X (DM) fails to match the same downward-shift in resonance to near 20 MHz, which exists in both experimental measurements. The shift of this resonance is representative of an increase in effective inductance

in the  $Y$  capacitor branch, which may be a result of unmodeled inductive coupling between the  $X$  and  $Y$  capacitors. The important similarity between the experimental measurements and the simulation is seen comparing Optimal  $Y$ , Uncanceled  $X$  (DM) and the final trace Optimal  $Y$ , Optimal  $X$  (DM). By appropriately locating the  $X$  capacitor on the coil, it is possible to both shift the resonance higher in frequency, and to increase the attainable attenuation.

If consideration is given to modeling the increase in effective inductance in the  $Y$  capacitor branch when the  $X$  capacitor is present, significantly improved correlations between the experimental measurements and the model simulation result. If  $Z_{Y_{DM}} = 2[R_Y + (j\omega C_Y)^{-1} + j\omega(L_Y + 0.2L_Y)]$ , which represents a modest 20% increase in effective inductance, and slightly moving (by 1.5 mm) the tuning location of the  $X$  capacitor on the coil to yield a refined inductance matrix

$$L_{\text{coil}} = \begin{bmatrix} 36.52 & 42.62 & 0.563 \\ 42.29 & 222.4 & 9.091 \\ 0.563 & 9.091 & 5.432 \end{bmatrix} nH$$

the plot in Fig. 22 results. These results correlate significantly better than the case without the added effective inductance, although differences are still notable for Optimal  $Y$ , Uncanceled  $X$  (DM).

Given the substantial modeling simplifications used in creating these simulations (e.g., neglecting coil-to-coil and other mutual couplings, using simple numerical simulations to obtain coil inductances, etc.) the degree of accuracy of the model is striking, confirming its usefulness for understanding the behavior of such systems.

## V. CONCLUSION

The size and performance of EMI filters are often limited by their component parasitics, such as the equivalent series inductance of capacitors. Past work has shown that a coupled magnetic winding can be used to cancel the effects of a single capacitor's parasitic inductance, thereby substantially improving filter performance.

This paper has built on previous work by demonstrating the use of a single coupled magnetic winding to compensate for the effects of the parasitic inductances of two discrete capacitors. This work was applied experimentally to both test filters and to a commercially-available EMI filter with great success. Further, the coupling of closely oriented magnetic windings was also investigated, illustrating their successful use in constrained spaces, and a possible avenue for optimizing winding size. Finally, an analytical basis for the inductance compensation is developed and compared to experimental results.

## APPENDIX

### THREE-PORT TAPPED-INDUCTOR EXTENDED CANTILEVER MODEL TRANSFER FUNCTION

Equation (10) gives the analytic solution of the transfer function from input voltage  $V_{in}$  to output voltage  $V_l$  for the circuit in Fig. 19. The result was found using direct circuit analysis, with the source network consisting of an input voltage source

$V_{in}$  with series impedance  $z_s$ , and a load network comprised of an impedance  $z_l$ .  $T_2$  and  $T_3$  are arbitrary impedances representing the two capacitors

$$H(s) = \frac{(T_2 T_3 - Z_{13} T_3 - Z_{12} T_3 - Z_{23} T_2 - Z_{13} T_2 + Z_{12} Z_{23} - Z_{13} Z_{22}) z_l}{T_3 z_l z_s + T_2 z_l z_s + Z_{22} z_l z_s + T_2 T_3 z_s + Z_{33} T_3 z_s + 2Z_{23} T_3 z_s + Z_{22} T_3 z_s + Z_{33} T_2 z_s + Z_{22} Z_{33} z_s - Z_{23}^2 z_s + T_2 T_3 z_l + Z_{11} T_3 z_l + Z_{22} T_2 z_l + 2Z_{12} T_2 z_l + Z_{11} T_2 z_l + Z_{11} Z_{22} z_l - Z_{12}^2 z_l + Z_{33} T_2 T_3 + 2Z_{23} T_2 T_3 + Z_{22} T_2 T_3 + 2Z_{13} T_2 T_3 + 2Z_{12} T_2 T_3 + Z_{11} T_2 T_3 + Z_{11} Z_{33} T_3 + 2Z_{11} Z_{23} T_3 + Z_{11} Z_{22} T_3 - Z_{13}^2 T_3 - 2Z_{12} Z_{13} T_3 - Z_{12}^2 T_3 + Z_{22} Z_{33} T_2 + 2Z_{12} Z_{33} T_2 + Z_{11} Z_{33} T_2 - Z_{23}^2 T_2 - 2Z_{13} Z_{23} T_2 - Z_{13}^2 T_2 + Z_{11} Z_{22} Z_{33} - Z_{12}^2 Z_{33} - Z_{11} Z_{23}^2 + 2Z_{12} Z_{13} Z_{23} - Z_{13}^2 Z_{22}} \quad (10)$$

## ACKNOWLEDGMENT

The authors would like to thank M. Comer, P. Ott, and E. Kloczkowski, Corcom Products Division, Tyco Electronics, for their generosity and assistance with aspects of this research.

## REFERENCES

- [1] T. K. Phelps and W. S. Tate, "Optimizing passive input filter design," in *Proc. 6th Nat. Solid-State Power Conv. Conf.*, May 1979, pp. G1.1–G1.10.
- [2] H. W. Ott, *Noise Reduction Techniques in Electronic Systems*, 2nd ed. New York: Wiley, 1988.
- [3] C. Sullivan and A. Kern, "Capacitors with fast current switching require distributed models," in *Proc. IEEE Power Electron. Spec. Conf.*, Vancouver, BC, Canada, Jun. 2001, vol. 3, pp. 1497–1503.
- [4] T. Uchida, T. Y. Katsuyuki, K. Sugitani, and K. Masami, "LC Filter With Capacitor Electrode Plate Not Interfering With Flux of Two Coils," U.S. Patent 6476 689, Nov. 5, 2002.
- [5] T. Neugebauer, J. Phinney, and D. Perreault, "Filters and components with inductance cancellation," *IEEE Trans. Ind. Appl.*, vol. 40, no. 2, pp. 483–491, Mar./Apr. 2004.
- [6] T. Neugebauer and D. Perreault, "Filters with inductance cancellation using printed circuit board transformers," *IEEE Trans. Power Electron.*, vol. 19, no. 3, pp. 591–602, May 2004.
- [7] D. Perreault, J. Phinney, and T. Neugebauer, "Filter Having Parasitic Inductance Cancellation," U.S. Patent 6937 115, Aug. 30, 2005.
- [8] S. Wang, F. Lee, D. Chen, and W. Odendaal, "Effects of parasitic parameters on emi filter performance," *IEEE Trans. Power Electron.*, vol. 19, no. 3, pp. 869–877, May 2004.
- [9] S. Wang, F. Lee, and W. Odendaal, "Using a network method to reduce the parasitic parameters of capacitors," in *Proc. IEEE Power Electron. Spec. Conf.*, Jun. 2004, vol. 1, pp. 304–308.
- [10] S. Wang, F. Lee, W. Odendaal, and J. van Wyk, "Improvement of emi filter performance with parasitic coupling cancellation," *IEEE Trans. Power Electron.*, vol. 20, no. 5, pp. 1221–1228, Sep. 2005.
- [11] T. Neugebauer and D. Perreault, "Parasitic capacitance cancellation in filter inductors," in *Proc. IEEE Power Electron. Spec. Conf.*, Jun. 2004, vol. 4, pp. 3102–3107.
- [12] R. Chen, J. van Wyk, S. Wang, and W. Odendaal, "Improving the characteristics of integrated emi filters by embedded conductive layers," *IEEE Trans. Power Electron.*, vol. 20, no. 3, pp. 611–619, May 2005.
- [13] A. Kamon, L. Silveira, C. Smithhisler, and J. White, *FastHenry USER'S GUIDE*, 3rd ed. Cambridge, MA: MIT, Nov. 1996.
- [14] *CORCOM Product Guide Catalog 1654001*. Libertyville, IL: Tyco Electronics, Mar. 2004.
- [15] D. Maksimovic, R. Erickson, and C. Griesbach, "Modeling of cross-regulation in converters containing coupled inductors," *IEEE Trans. Power Electron.*, vol. 15, no. 4, pp. 607–615, Jul. 2000.

- [16] K. Changtong, R. Erickson, and D. Maksimovic, "A comparison of the ladder and full-order magnetic models," in *Proc. IEEE Power Electron. Spec. Conf.*, Vancouver, BC, Canada, Jun. 2001, vol. 4, pp. 2067–2071.
- [17] J. Hayes, N. O'Donovan, and M. Egan, "The extended t model of the multiwinding transformer," in *Proc. IEEE Power Electron. Spec. Conf.*, Jun. 2004, vol. 3, pp. 1812–1817.
- [18] K. Ngo, S. Srinivas, and P. Nakmahachalasint, "Broadband extended cantilever model for magnetic component windings," *IEEE Trans. Power Electron.*, vol. 16, no. 4, pp. 551–557, Jul. 2001.
- [19] K. Ngo and A. Gangupomu, "Improved method to extract the short-circuit parameters of the becm," *IEEE Power Electron. Lett.*, vol. 1, no. 1, pp. 17–18, Jan. 2003.



**Brandon J. Pierquet** (S'03) received the B.S. degree in electrical engineering from the University of Wisconsin, Madison, in 2004 and the S.M. degree from the Massachusetts Institute of Technology (MIT), Cambridge, in 2006, where he is currently pursuing the Ph.D. degree in the Laboratory for Electromagnetic and Electronic Systems.

He is currently a Research Assistant in the Laboratory of Electromagnetic and Electronic Systems, MIT.



**Timothy C. Neugebauer** (M'04) received the B.S. degree in electrical engineering from Union College, Schenectady, NY in 1997, and the M.S. and Ph.D. degrees from the Massachusetts Institute of Technology, Cambridge, in 1999 and 2004, respectively.

He currently works for Draper Laboratories, Cambridge.



**David J. Perreault** (S'91–M'97–SM'05) received the B.S. degree from Boston University, Boston, MA, in 1989, and the S.M. and Ph.D. degrees from the Massachusetts Institute of Technology (MIT), Cambridge, in 1991 and 1997, respectively.

In 1997 he joined the MIT Laboratory for Electromagnetic and Electronic Systems as a Postdoctoral Associate, and became a Research Scientist in the laboratory in 1999. In July 2001, he joined the MIT Department of Electrical Engineering and Computer Science, where he is presently the Emanuel

E. Landsman Associate Professor of Electrical Engineering and Computer Science. His research interests include design, manufacturing, and control techniques for power electronic systems and components, and in their use in a wide range of applications.

Dr. Perreault received the Richard M. Bass Outstanding Young Power Electronics Engineer Award from the IEEE Power Electronics Society, an ONR Young Investigator Award, the SAE Ralph R. Teeter Educational Award, and has two IEEE prize paper awards. He is a member of Tau Beta Pi and Sigma Xi.